Stability of Sr adatom model structures for $SrTiO_3$(001) surface reconstructions

2005 J. Phys.: Condens. Matter 17 L223

(http://iopscience.iop.org/0953-8984/17/23/L01)

INSTITUTE OF PHYSICS PUBLISHING JOURNAL OF PHYSICS: CONDENSED MATTER

J. Phys.: Condens. Matter **17** (2005) L223–L230 doi:10.1088/0953-8984/17/23/L01

LETTER TO THE EDITOR

Stability of Sr adatom model structures for $SrTiO_3$(001) surface reconstructions

Leandro M Liborio, Cristián G Sánchez, Anthony T Paxton and Michael W Finnis

Atomistic Simulation Centre, School of Mathematics and Physics, Queen's University Belfast, Belfast BT7 1NN, UK

Received 21 March 2005, in final form 2 May 2005
Published 27 May 2005
Online at stacks.iop.org/JPhysCM/17/L223

Abstract

We report results of first-principles calculations on the thermodynamic stability of different Sr adatom structures that have been proposed to explain some of the observed reconstructions of the (001) surface of strontium titanate (Kubo and Nozoye 2003 *Surf. Sci.* **542** 177). From surface free energy calculations, a phase diagram is constructed indicating the range of conditions over which each structure is most stable. These results are compared with Kubo and Nozoye's experimental observations. It is concluded that low Sr adatom coverage structures can only be explained if the surface is far from equilibrium. Intermediate coverage structures are stable only if the surface is in or very nearly in equilibrium with the strontium oxide.

1. Introduction

The surface structure and properties of $SrTiO_3$, considered as a prototype for oxides with the perovskite structure, have been studied extensively [2–6]. $SrTiO_3$ has been used as a substrate for the growth of high T_c superconducting thin films [7] and it has also been investigated as a buffer material for the growth of GaAs on Si [8]. But in spite of the scientific and technological relevance of $SrTiO_3$, its surface atomic structure and its reconstructions are only poorly understood.

It is immediately obvious from the literature that a very rich proliferation of surface reconstructions exists, in a variety of stoichiometries. Under oxidizing conditions at ambient pressure, (2×1) and $c(4 \times 2)$ surface reconstructions are reported [9, 10, 6, 5]; whereas after annealing in vacuum under reducing conditions [4, 1] further structures have been observed. Many reconstructions have been attributed to ordering of oxygen defects [11–13]. However, several theoretical results for this model are inconsistent with experimental results [14, 15]. These inconsistencies have led to the belief that the behaviour of the (001) surface of $SrTiO_3$ cannot be described by a standard point defect model in terms of only oxygen vacancies. Additional models have been proposed by Erdman [6, 5] and Castell [4]. The former explained

SrO-deficient surface structures of $SrTiO_3(001)$ through surface rearrangements of TiO_{6-x} units into edge-sharing blocks, while the latter removed alternate rows of oxygen from the (1×1) TiO_2 terminated surface in order to create a surface with a reduced stoichiometry and a (2×1) surface unit cell. The model that we concentrate upon in the present work is the so-called *Sr adatom model*, which consists of an ordered array of Sr adatoms at oxygen fourfold sites of a TiO_2 terminated layer. This model was first proposed for the $(\sqrt{5} \times \sqrt{5})$-R26.6° reconstruction by Kubo and Nozoye [16], and these authors in a later paper [1] used this model to explain almost all the reported $SrTiO_3(001)$ surface reconstructions.

Given this perplexing array of observations, a natural question to ask is which, if any, of these structures is in equilibrium; and if the surface is in equilibrium, is it with the underlying bulk crystal, with the surrounding gas phase, or with some other metal or oxide phase? Here we address these questions by analysing the thermodynamic stability of the different Sr adatom structures proposed in [1] by calculating their surface free energies from first principles under a variety of experimental conditions. We construct a phase diagram indicating the conditions over which each structure is most stable. Finally we compare our results with Kubo and Nozoye's experimental observations.

2. Method of total energy calculations

Our calculations were performed within the local density approximation [17, 18] to density functional theory [19, 20] as implemented in the SIESTA program [21, 22]. The effect of core electrons was taken into account through norm-conserving fully separable Troullier–Martins pseudopotentials [23]. Due to the large overlap between the semi-core and valence states, the 3s and 3p electrons of Ti together with the 4s and 4p electrons of Sr were explicitly included in the calculation. The cut-off radii and reference configurations used to generate the pseudopotentials were obtained from [24].

A basis of numerical atomic orbitals, generated using the methods described in [25], was used to expand the one-electron Kohn–Sham orbitals. A single-ζ basis set was used for the semi-core states of Ti and Sr, and a double-ζ plus a single shell of polarization functions for the valence states of all atoms. The localization radii and ionic charges used to generate the basis orbitals were taken from [26].

Obtaining the matrix elements of the Hartree and exchange and correlation parts of the Hamiltonian was performed numerically on a uniform real space grid [21] with a spacing equivalent to a plane-wave cut-off of 200 Ryd. Once self-consistency was achieved, the grid spacing was halved in order to compute the total energy and atomic forces. Sampling of reciprocal space was done with a $(6 \times 6 \times 6)$ Monkhorst–Pack mesh for the bulk unit cell of $SrTiO_3$ and an equivalent quality mesh [27] for bulk SrO and TiO_2 and all slabs used to represent the surfaces. Further increasing the size of the reciprocal space mesh produced changes in the surface energies of the SrO and TiO_2 terminated (1×1) surfaces of less than 0.04 J m^{-2}.

Results for the lattice constant, bulk modulus and elastic constants of bulk $SrTiO_3$ are shown in table 1. Our present results are in good agreement with previous theoretical and experimental results. The calculated lattice constant of $SrTiO_3$ was used for all slabs representing the surfaces.

All surface structures were represented by periodically repeated symmetric slabs consisting of seven intercalated layers of TiO_2 and SrO separated by a vacuum space of three lattice constants. All atomic positions within the outermost three layers were fully relaxed in all cases. Test calculations with (1×1) SrO and TiO_2 terminated slabs, having a number of layers ranging from 7 up to 19, and a vacuum region up to five lattice constants, showed

Table 1. Results obtained for the lattice constant (a), bulk modulus (B) and elastic constants (C_{44} and C') of bulk $SrTiO_3$ compared with existing results obtained from experiment [28], the full-potential linear muffin tin orbitals method (FP-LMTO) [29] and the pseudopotential plane-waves method (PWP) [30].

Method	a (Å)	B (GPa)	C_{44} (GPa)	C' (GPa)
Experimental	3.91	184	128	119
Present work	3.87	203	121	142
FP-LMTO	3.85	200	125	140
PWP	3.86	200	155	142

variations of the surface energy smaller than 0.01 J m^{-2}. Allowing the relaxation of more than the three outermost layers resulted in a variation of the surface free energy of less than 0.02 J m^{-2} in all cases.

3. Calculation of the surface energy

The relative stability of the different surface reconstructions is determined by their surface free energy. Under given conditions, the most stable surface will be that of lowest surface free energy. The formalism used here to calculate surface free energies for different stoichiometries has been described in detail by one of us in [31]. This method has been used in the past to study the reconstructions of GaAs surfaces [32, 33], and the phase diagram for H adsorption on GaN surfaces [34].

For a particular surface structure the surface free energy was calculated as follows. We have a slab of crystal displaying two surfaces to which we apply periodic boundary conditions in the usual way. We choose three components to be SrO, TiO_2 and O and to describe the stoichiometry we express the number of each of these components in terms of their thermodynamic excess with respect to one of the three. The excess of component i with respect to component A is

$$\Gamma_i = \frac{1}{2A_s}\left(N_i - N_A \frac{N_i^{\text{bulk}}}{N_A^{\text{bulk}}}\right). \tag{1}$$

We arbitrarily refer our excesses to SrO in which case the surface free energy is

$$\sigma = \frac{1}{2A_s}(G_s - N_{SrO} g_{SrTiO_3}) - \mu_{TiO_2}\Gamma_{TiO_2} - \frac{1}{2}\mu_{O_2}\Gamma_O \tag{2}$$

where A_s is the area of one of the surfaces of the slab, G_s its free energy and g_{SrTiO_3} the free energy of bulk $SrTiO_3$ per formula unit. μ_{TiO_2} and μ_{O_2} are the chemical potentials of TiO_2 and O_2 respectively. According to the phase rule, since the system consists of two phases and three components, three degrees of freedom exist that must be fixed to fully determine its state. For convenience these are chosen to be μ_{TiO_2}, the temperature T and the oxygen partial pressure p_{O_2}. The temperature and pressure dependence of the free energies and chemical potentials of all condensed phases were neglected. For all of these, the free energy was calculated from the total energy at zero temperature using the method described in section 2. The numbers of units of each component for the slabs representing the different surfaces are shown in table 2.

The condition that the slab be stable with respect to decomposition into its components imposes limits on the allowed ranges of variation of temperature, oxygen partial pressure and the chemical potential of TiO_2. The chemical potentials of both SrO and TiO_2 must be below their respective bulk values otherwise these components would precipitate and the slab would decompose. The definitions of Gibbs energy and chemical potentials require

$$g_{SrTiO_3} = \mu_{TiO_2} + \mu_{SrO} \tag{3}$$

Table 2. N_{SrO}, Γ_{TiO_2} and Γ_O for the slabs representing the different surface structures. $A_s^{(1\times1)}$ is the area of one of the surfaces of a (1×1) terminated slab. θ_{Sr} is the coverage of Sr in the adatom model and T^E is the experimental temperature at which the surface reconstruction was observed in [1].

Surface	N_{SrO}	$A_s^{(1\times1)}\Gamma_{TiO_2}$	$A_s^{(1\times1)}\Gamma_O$	θ_{Sr}	T^E (°C)
(1×1) TiO_2	3	$\frac{1}{2}$	0	0	Not observed
$(\sqrt{13} \times \sqrt{13})$	28	$\frac{11}{26}$	$-\frac{1}{13}$	0.0769	1250
$c(4 \times 4)$	18	$\frac{3}{8}$	$-\frac{1}{8}$	0.125	1100
$(\sqrt{5} \times \sqrt{5})$	12	$\frac{3}{10}$	$-\frac{1}{5}$	0.2	1200
(2×2)	10	$\frac{1}{4}$	$-\frac{1}{4}$	0.25	1000
$c(4 \times 4)$	22	$\frac{1}{8}$	$-\frac{3}{8}$	0.375	1000

and combined with the energy of formation of $SrTiO_3$

$$\Delta G_{f,SrTiO_3} = g_{SrTiO_3} - \mu^{bulk}_{TiO_2} - \mu^{bulk}_{SrO} \tag{4}$$

the stability of the slab imposes the following limits on the chemical potential of TiO_2:

$$\mu^{bulk}_{TiO_2} + \Delta G_{f,SrTiO_3} \leqslant \mu_{TiO_2} \leqslant \mu^{bulk}_{TiO_2}. \tag{5}$$

By similar reasoning, requiring that the chemical potential of each of the metals in our system be less than its bulk value imposes limits on the oxygen chemical potential as follows:

$$2\mu_O(p_{O_2}, T) \geqslant \mu_{TiO_2} - \mu^{bulk}_{Ti} \tag{6}$$

$$\mu_O(p_{O_2}, T) \geqslant g_{SrTiO_3} - \mu_{TiO_2} - \mu^{bulk}_{Sr}. \tag{7}$$

For the range of temperatures considered here, it is the first of this equations that sets the lower limit of μ_O. This limit is represented in the phase diagrams shown in figures 1(a) and (b) as a forbidden region of temperatures and pressures.

The oxygen chemical potential was calculated as described in [35]. First, the value of the chemical potential of oxygen is calculated at standard temperature and pressure from the experimental formation Gibbs free energy of a series of oxides, and the calculated free energies of their condensed phase components. The standard chemical potential of oxygen used in this work was calculated as the average of those obtained from the Gibbs energies of formation of the oxides: SrO, TiO_2, MgO, SiO_2, Al_2O_3, CaO, PbO_2, CdO, SnO_2, Cu_2O, Ag_2O and ZnO. The value obtained was $\mu^0_{O_2} = -433.23$ eV/molecule. A standard deviation of 0.44 eV/molecule is associated with this value which is related to the systematic omission of the thermal contributions to the free energies and the local density and pseudopotential approximations [31]. This uncertainty in $\mu^0_{O_2}$ translates into an uncertainty in the positions of the phase boundaries in figures 1(a) and (b) which depends on temperature as

$$\Delta \log p_{O_2} = -0.43\frac{\Delta\mu^0_{O_2}}{k_B T} \tag{8}$$

which varies between 1.9 and 2.85. The uncertainty in $\mu^0_{O_2}$ cannot affect our predicted ordering of reconstructions as a function of T or p_{O_2}.

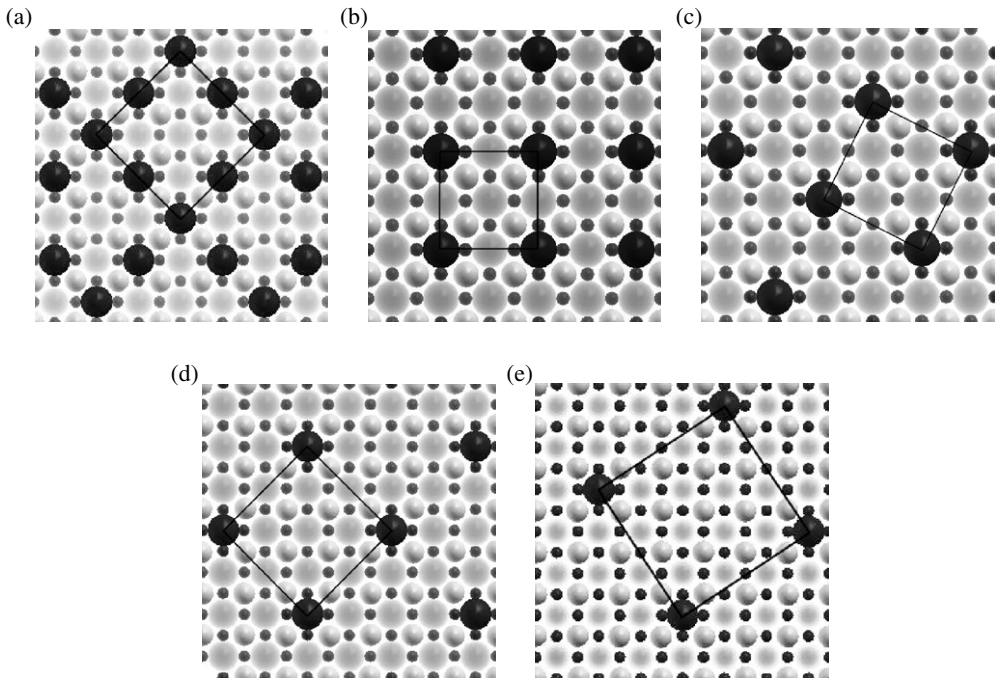

Figure 1. Top views of the Sr adatom model surface structures listed in table 2. The black circles represent Sr adatoms and the surface unit cell is indicated in each reconstruction. The clean TiO_2 terminated surface is the atomic layer below each reconstruction and is shown as a foggy background. (a) c(4 × 4), $\theta = 0.375$, (b) (2 × 2), $\theta = 0.25$, (c) $(\sqrt{5} \times \sqrt{5})$, $\theta = 0.20$, (d) c(4 × 4), $\theta = 0.125$, (e) $(\sqrt{13} \times \sqrt{13})$, $\theta = 0.0769$.

4. Results and discussion

Using equation (2) we calculated the surface energies of all of the Sr adatom structures proposed by Kubo and Nozoye in [1] (listed in table 2) for the allowed ranges of the variables μ_{TiO_2}, p_{O_2} and T. The atomic structure of these reconstructions is shown in figure 1. Phase diagrams were constructed by finding the most stable surface for each set of conditions. Limits on the μ_{TiO_2} are set by equation (5). Figure 2(a) shows the phase diagram with μ_{TiO_2} at its lower limit. Figure 2(b) shows the phase diagram with μ_{TiO_2} at its upper limit. At the lower limit for μ_{TiO_2}, the value of μ_{SrO} is at its maximum and the surface is in equilibrium with bulk SrO. As can be seen from the figure, at high p_{O_2} and low T the clean TiO_2 terminated surface is the most stable. Upon increasing T or lowering the p_{O_2}, the Sr covered surfaces progressively decrease in surface energy, becoming more stable than the TiO_2 terminated surface. The equilibrium Sr coverage increases with increasing T and decreasing p_{O_2}. In the limit of stability of the slab, the most stable of the proposed surfaces is the one with a Sr coverage of $\theta = 0.25$ monolayers. The higher coverage structures are never stable in the allowed region, the $\theta = 0.375$ c(4 × 4) structure lying just within the border of the forbidden region.

Figure 3 shows the phase diagram in a construction proposed by Van de Walle and Neugebauer [34]. In this case the independent variables are μ_{TiO_2} and μ_O. As μ_O decreases it can be seen that the Sr coverage increases.

This ordering of the stability can be explained by taking into account that SrO in the slab is in equilibrium with Sr atoms at the surface and O_2 in the gas phase:

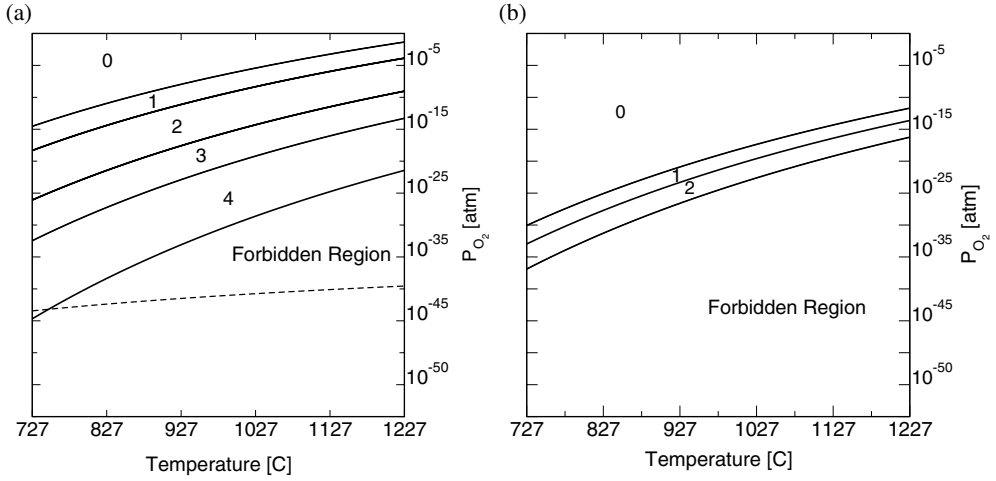

Figure 2. Surface phase diagram for the different Sr adatom structures as a function of temperature and partial oxygen pressure. Continuous lines separate the regions in which each structure is stable; the dashed line in figure (a) indicates the oxygen partial pressure in equilibrium with solid C. The surfaces are denoted as follows: (0): TiO_2 terminated (1×1); (1): $(\sqrt{13} \times \sqrt{13}), \theta = 0.0769$; (2): $c(4 \times 4), \theta = 0.125$; (3): $(\sqrt{5} \times \sqrt{5}), \theta = 0.20$; (4): $(2 \times 2), \theta = 0.25$.

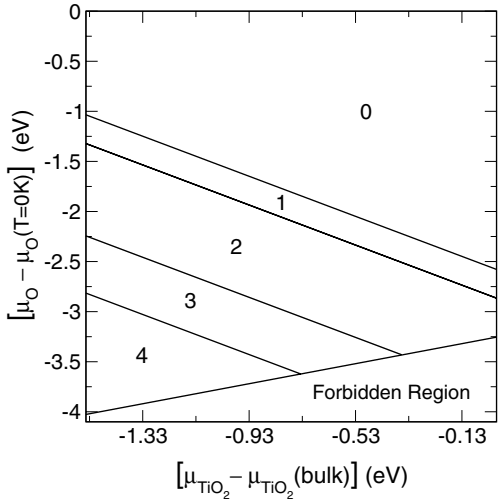

Figure 3. Surface phase diagram for the different Sr adatom structures as a function of μ_O and μ_{TiO_2}.

$$\mathrm{SrO\ (slab)} \rightleftharpoons \mathrm{Sr\ (surface)} + \tfrac{1}{2}\mathrm{O_2\ (gas)}. \tag{9}$$

Therefore the chemical potentials of O_2 and Sr are related by

$$\mu_{SrO} = \mu_{Sr} + \tfrac{1}{2}\mu_{O_2}. \tag{10}$$

Increasing the temperature or lowering the p_{O_2} lowers the μ_{O_2}. Similarly a decrease in coverage of Sr in the surface lowers the μ_{Sr}. For a given μ_{SrO}, decreasing the μ_{O_2} increases the μ_{Sr}, allowing the appearance of higher coverage phases. In other words, lowering the p_{O_2} displaces the equilibrium in equation (9) to the right, increasing the Sr coverage. Upon decreasing the

μ_{SrO}, the maximum value of μ_{Sr} that can be achieved before reaching the forbidden region is lower and only the lower coverage surfaces are accessible.

In [1] the authors obtained a TiO_2 terminated surface by chemical etching. After annealing at 1000 °C the authors observed clusters coexisting with what they interpret as $\theta = 0.375$ c(4 × 4) and $\theta = 0.25$ (2 × 2) domains. On annealing the sample at increasing temperatures up to 1100 °C they observed a decrease in coverage to $\theta = 0.125$, as the surface transformed to the second c(4 × 4) structure. Disordered phases were also observed in the process. A further increase in temperature to 1180 °C led to a further apparent reduction in coverage to $\theta = 0.0625$ and the formation of a 4 × 4 structure that we have not studied. Raising the temperature further to 1200 °C and 1250 °C led first to an increase in coverage as the $\theta = 0.2(\sqrt{5} \times \sqrt{5})$ surface formed, followed by an apparent decrease in coverage to $\theta = 0.0769$ as suggested by the $(\sqrt{13} \times \sqrt{13})$ structure.

According to our results, high Sr adatom coverages can only be achieved when the surface is (or is close to being) in equilibrium with SrO, near the lower limit of the TiO_2 chemical potential. Kubo and Nozoye's interpretation of the observed clusters being composed of SrO_x-type compounds might suggest that this is the case. Another condition that our phase diagram indicates is the extremely low effective partial pressure of oxygen that can be achieved if a reducing agent is present [35]. Kubo and Nozoye's preparation method uses a chemical etch that is known to leave a carbon residue [3]. In figure 1(a) the dashed line indicates the oxygen partial pressure in equilibrium with solid C as a function of temperature[1]. At 726.85 °C and for this oxygen pressure the $\theta = 0.25$ (2 × 2) structure is the most stable. At higher temperatures, but within the forbidden region, the $\theta = 0.375$ (4 × 4) case would be in equilibrium with a metastable substrate. At temperatures above 726.85 °C the lower coverage surfaces are only stable at oxygen pressures well above the 5×10^{-12} atm limit.

Although the $\theta = 0.375$ c(4 × 4) and $\theta = 0.25$ (2 × 2) structures might be obtained at equilibrium or near equilibrium, all lower coverage structures are unstable at the experimentally accessible conditions, with the exception of the $(\sqrt{5} \times \sqrt{5})$, $\theta = 0.20$ structure which is stable in a narrow pressure region below the ultrahigh vacuum (UHV) pressure at the temperatures reported by Kubo and Nozoye. Kubo and Nozoye proposed the evaporation of Sr from the surface with increasing temperature as an explanation of the decrease in coverage with temperature, and supported this with calculations of the energy required to desorb Sr atoms. Our results support their interpretation if we also assume that there is no equilibration of the surface with the gas phase.

5. Conclusions

We have performed first-principles total energy calculations for several Sr adatom structures proposed by Kubo and Nozoye as models for the reconstructions of the (001) surface of $SrTiO_3$ [1]. The surface energies were calculated as a function of TiO_2 chemical potential, temperature and oxygen partial pressure for the conditions under which the substrate is thermodynamically stable. The results were used to construct a surface phase diagram showing the range of stability of each structure. Only surfaces with coverages of $\theta = 0.25$ and 0.20 are stable for the ranges of temperature and pressure reported in [1] and only when the substrate is in or very nearly in equilibrium with SrO. The other structures observed have been interpreted in a plausible way by Kubo and Nozoye within the same sequence of Sr adatom models. Our

[1] This pressure was calculated taking into account all equilibria between C, CO, CO_2 and O_2 using values for the gas reaction free energies obtained from [36]. A total pressure of 5×10^{-12} atm was used, which is the value reported as a higher limit during annealing in [1].

calculations show that the lower Sr coverages implied by these models can only be explained if the surface is far from equilibrium, in a transient state as it loses Sr to the environment.

We thank the EPSRC for support of this work under grant GR/R39085/01.

References

[1] Kubo T and Nozoye H 2003 *Surf. Sci.* **542** 177
[2] Akiyama R, Matsumoto T, Tanaka H and Kawai T 1997 *Japan. J. Appl. Phys.* **36** 3881
[3] Kawasaki M, Takahashi K, Maeda T, Tsushiya R, Shinohara M, Ishiyama O, Yonezawa T M Y and Koinuma H 1994 *Science* **266** 1540
[4] Castell M R 2002 *Surf. Sci.* **505** 1
[5] Erdman N, Warschkow O, Asta M, Poeppelmeier K R, Ellis D E and Marks L D 2003 *J. Am. Chem. Soc.* **125** 10050
[6] Erdman N, Poeppelmeier K R, Asta M, Warshkow O, Ellis D E and Marks L D 2002 *Nature* **419** 55
[7] Aruta C *et al* 2001 *Phys. Status Solidi* a **183** 353
[8] Droopard R, Yu Z, Ramdani J, Hilt L, Curless J, Overgaard C, Edwards J L Jr, Finder J, Eisenbeiser K and Ooms W 2001 *Mater. Sci. Eng.* B **87** 292
[9] Cord B and Courths R 1985 *Surf. Sci.* **162** 34
[10] Jiang Q D and Zegenhagen J 1999 *Surf. Sci.* **425** 343
[11] Tanaka H, Matsumoto T, Kawai T and Kawai S 1993 *Japan. J. Appl. Phys.* **32** 1405
[12] Haruyama H, Koderira S, Aiura Y, Bando H, Nishiara Y, Maruyama T and Sakisaka Y 1996 *Phys. Rev.* B **53** 8032
[13] Courths R, Koffke J, Wern H and Heise R 1990 *Phys. Rev.* B **42** 9127
[14] Kimura S, Yamauchi J, Tsukada M and Watanabe S 1995 *Phys. Rev.* B **51** 11049
[15] Kimura S and Tsukada M 1997 *Appl. Surf. Sci.* **121/122** 195
[16] Kubo T and Nozoye H 2001 *Phys. Rev. Lett.* **86** 1801
[17] Perdew J P and Zunger A 1981 *Phys. Rev.* B **23** 5048
[18] Ceperley D M and Alder B J 1980 *Phys. Rev. Lett.* **45** 566
[19] Hohenberg P and Kohn W 1964 *Phys. Rev.* **136** B864
[20] Kohn W and Sham L J 1965 *Phys. Rev.* **140** A1133
[21] Soler J M, Artacho E, Gale J D, García A, Junquera J, Ordejón P and Sánchez-Portal D 2002 *J. Phys.: Condens. Matter* **14** 2745
[22] Ordejón P, Artacho E and Soler J M 1996 *Phys. Rev.* B **53** R10441
[23] Troullier N and Martins J 1991 *Phys. Rev.* B **43** 1993
[24] Junquera J, Zimmer M, Ordejón P and Ghosez P 2003 *Phys. Rev.* B **67** 155327
[25] Soler J M, Artacho E, García A, Ordejón P and Sánchez-Portal D 1999 *Phys. Status Solidi* b **215** 809
[26] Ordejón P, Artacho E, Cachau R, Gale J, García A, Junquera J, Kohanoff J, Machado M, Sánchez-Portal D, Soler J M and Weht R 2001 *Mater. Res. Soc. Symp. Proc.* **677** AA9.6.1
[27] Moreno J and Soler J M 1992 *Phys. Rev.* B **45** 13891
[28] *Landolt–Börnstein* Group III *Condensed Matter* 2002 vol 36, subvol V (Berlin: Springer) chapter 1A (Simple Perovskyte-Type Oxides) pp 116–47
[29] Johnston K 2003 Atomic scale modeling of strontium titanate *PhD Thesis* Queen's University Belfast
[30] King-Smith R D and Vanderblit D 1994 *Phys. Rev.* B **49** 5828
[31] Finnis M W, Lozovoi A Y and Alavi A 2005 *Annu. Rev. Mater. Res.* at press
[32] Qian G, Martin R and Chadi D J 1988 *Phys. Rev. Lett.* **60** 1962
[33] Esser N, Shkrebtii A I, Resch-Esser U, Springer C, Richter W, Schmidt W G, Bechstedt F and Sole R D 1996 *Phys. Rev. Lett.* **77** 4402
[34] Van de Walle C G and Neugebauer J 2002 *Phys. Rev. Lett.* **88** 066103
[35] Johnston K, Castell M, Paxton A T and Finnis M W 2004 *Phys. Rev.* B **70** 085415
[36] Gaskell D R 1981 *Introduction to Metallurgical Thermodynamics* (*McGraw-Hill Series in Materials Science and Engineering*) (New York: McGraw-Hill)